



Assessing the impact of large volcanic eruptions of the Last Millennium on Australian rainfall regimes

Stephanie Blake^{a,b}, Sophie C. Lewis^{b,c} and Allegra N. LeGrande^d

5

^a Climate Change Research Centre, University of New South Wales, Sydney, UNSW, Australia

^b ARC Centre of Excellence for Climate System Science

^c Fenner School of Environment and Society, The Australian National University, Canberra, ACT, Australia

^d NASA Goddard Institute for Space Studies and Center for Climate Systems Research, Columbia University

10 *Corresponding author:* Stephanie Blake (stephanieblake79@gmail.com)

Abstract. Explosive volcanism is an important natural climate forcing, impacting global surface temperatures and regional precipitation. Although previous studies have investigated aspects of the impact of tropical volcanism on various ocean-atmosphere systems and regional climate regimes, volcanic eruptions remain a poorly understood climate forcing and climatic responses are not well constrained. In this study, volcanic eruptions are explored in particular reference to Australian precipitation, and both the Indian Ocean Dipole (IOD) and El Niño-Southern Oscillation (ENSO). Using nine realisations of the Last Millennium (LM) with different time-evolving forcing combinations, from the NASA GISS ModelE2-R, the impact of the 6 largest tropical volcanic eruptions of this period are investigated. Overall, we find that volcanic aerosol forcing increased the likelihood of El Niño and positive IOD conditions for up to four years following an eruption, and resulted in positive precipitation anomalies over northwest (NW) and southeast (SE) Australia. Larger atmospheric sulfate loading coincides with more persistent positive IOD and El Niño conditions, enhanced positive precipitation anomalies over NW Australia, and dampened precipitation anomalies over SE Australia.

25

1. Introduction

Volcanic eruptions have significant impacts on weather and climate variability through the injection of volcanogenic material into the atmosphere. Sulfate aerosols, formed through the reaction of SO₂ and OH⁻ in the volcanic cloud, decrease incoming shortwave radiation, and if injected into the stratosphere, can generate a global response (Driscoll et al., 2012; LeGrande et al., 2016). Previous studies have identified relationships between volcanism and surface and tropospheric cooling (Driscoll et al., 2012), local stratospheric warming (Wielicki et al., 2002), strengthening of the Arctic Oscillation and Atlantic meridional overturning circulation (Oman et al., 2005; Stenchikov et al., 2006, 2009 & Shindell et al., 2004), and negative global precipitation anomalies (Gillet et al., 2004). The present study focuses on the under-studied relationship between large, globally significant tropical eruptions in the Last Millennium (850-1850CE) and the El-Niño Southern Oscillation (ENSO), Indian Ocean Dipole (IOD) and Australian precipitation.

35

Previous studies have focused on the response of ENSO to volcanic eruptions. Adams et al. (2003) demonstrated a statistical relationship between explosive tropical volcanism and the ENSO; a tropical mode that has been linked to variations in Australian precipitation anomalies (Meyers et al., 2007; Pepler et al., 2014). They showed that large tropical eruptions can increase the likelihood and amplitude of an El Niño event in following years, followed by a weaker La Niña state. Further work by Mann et al. (2005), Emile-Geay et al. (2008), McGregor et al. (2010), Wahl et al. (2014) and Predybaylo et al. (2017) supported this result. Pausata et al. (2015) identified that a radiative forcing threshold value of more than 15 W m⁻² is required to affect the ENSO, and that high latitude Northern Hemisphere

40



45 eruptions, in addition to tropical eruptions, are capable of doing so, as long as the forcing is asymmetric with regards to the equator.

The relationship between volcanic forcing and ENSO has been attributed to two contrasting, though not unrelated, mechanisms. The dynamical thermostat mechanism (Clement et al., 1996), whereby a uniform reduction of the surface
50 heat flux due to volcanism causes warming of the eastern equatorial Pacific, was identified as the driver of ENSO's response to volcanism by Mann et al. (2005) and Emile-Geay et al. (2008). Conversely, a shift in the Intertropical Convergence Zone (ITCZ) induced by strong radiative forcing, was accredited in more recent studies (Pausata et al., 2015; Stevenson et al., 2016). Preconditioning does impact the severity of the ENSO response. Predybaylo et al. (2017) found that years with an initial central Pacific El Nino ENSO phase show the largest statistical impact from Pinatubo-sized eruptions and that summer eruptions coincided with a more pronounced El Nino response.
55

Despite the understanding that volcanism can trigger or amplify El Nino events in the following years, the exact relationship between ENSO and volcanic forcing is still debated. McGregor and Timmermann (2011) and Zanchettin et al. (2012) reported an enhanced probability of La Nina events occurring in the immediate years after a volcanic
60 eruption, rather than El Nino, while several other studies (Self et al., 1997; Robock, 2000; Ding et al., 2014) found no relationship between ENSO and volcanic forcing. Robock (2000) argued that both El Chichon and Pinatubo reached their peak forcing after the initiation of El Nino events, indicating a coincidental relationship, while other studies (Driscoll et al., 2012; Lewis & Karoly, 2014; Lewis & LeGrande, 2015; Predybaylo et al., 2017) have pointed out challenges in determining long-term characteristics of ENSO due to short instrumental records, and its relationship to volcanic forcing due to variable representations of both ENSO and volcanic aerosols in GCMs (Global Climate
65 Models).

Comparatively little research has gone into the effects of volcanic forcing on the Indian Ocean Dipole (IOD), despite its known climatic impacts on Indian Ocean basin countries, such as Australia, South Africa, India and Indonesia (Cheung & Abram, 2016). The IOD is the zonal SST gradient between the tropical western Indian Ocean (WIO) and the tropical south eastern Indian Ocean (EIO) (Roxy et al., 2011), defined by the Dipole Mode Index (DMI). Cheung & Abram (2016) found that the DMI shows a statistically significant correlation to volcanic forcing, with a negative IOD (nIOD) occurring immediately after an eruption and a positive IOD (pIOD) one year later. Maher et al. (2015) found a similar relationship, with coinciding El Nino and pIOD events occurring 6-12 months after the peak of volcanic forcing. The
75 response of the IOD to volcanic forcing has been hypothesised to result from either the IOD's relationship with ENSO (Cheung & Abram, 2016), or the volcanically-induced reduction of the Asian Monsoon (Anchukaitis et al., 2010; Zambri et al., 2017).

Australian precipitation is affected by both the IOD and ENSO. Positive IOD (pIOD) and El Nino events typically
80 cause averaged precipitation deficits, while negative IOD (nIOD) events and La Nina cause positive precipitation anomalies (Meyers et al., 2007; Pepler et al., 2014). While ENSO is often held responsible for triggering Australian droughts, the IOD has been shown to have an equal, if not larger, impact on heavily populated areas of Australia, with all significant southeastern Australia droughts in the 20th C showing a larger response to pIOD events than El Ninos (Ummenhofer et al., 2009).

85



Volcanic aerosols have been found to cause global precipitation deficits for up to 5 years post-eruption (Robock & Lui, 1994; Iles et al., 2013; Gillett et al., 2004; Gu & Adler, 2011; Soden et al., 2002; Joseph & Zeng, 2011; Schneider et al., 2009; Timmreck et al., 2012; Iles et al., 2015). However, these deficits have been shown to vary seasonally (Joseph & Zeng, 2011), and cause positive precipitation anomalies over the NW and SE of Australia in the Southern Hemisphere (SH) winter and early spring (June-September), despite significant precipitation deficits in the summer (Joseph & Zeng, 2011; Schneider et al., 2009). Schneider et al. (2009) found a precipitation increase in the SH winter in Australia, Africa and Southern Asia. This current study explores these unclear relationships between volcanic eruptions and Australian rainfall.

95 2. Data and methods

2.1 Simulations

To understand the response of the IOD, ENSO and Australian precipitation towards volcanic forcing in the last millennium, we analysed 9 ensembles from the NASA GISS ModelE2-R (hereafter simply GISS) (Schmidt et al., 2014). The GISS ensemble was run for the pre-industrial part of the last millennium (LM), from 850-1850 CE, which is defined by the Coupled Model Intercomparison Project Phase 5 (CMIP5) (Taylor et al., 2012). GISS is run at 2 degrees x 2.5 degrees horizontal resolution, with 40 vertical levels up to 0.1 hPa.

Five ensembles were forced with volcanic forcing, while four were not. Of the five run with volcanic forcing, four were forced with Crowley and Unterman (2013)'s aerosol optical depth data (CR), and one with double the Ice-core Volcanic Index 2 by Gao et al. (2008) (2xG) (see Table 1 for experiment summary). The GISS model is forced with prescribed Aerosol Optical Depth (AOD) from 15-35 km. The LM simulations also include transient solar and land use histories that differ between ensembles. However, as this analysis focuses primarily on the immediate post-volcanic response, the impact of these smaller amplitude and slowly varying forcings is likely to be insignificant (Colose et al., 2016).

2.2 Methods

First, the six largest tropical eruptions between 850-1850CE were identified by the magnitude of their total global stratospheric sulfate aerosol injection (T_g) from the IVI2 Version 2 dataset, revised in 2012 (Gao et al., 2008), and the years surrounding eruption extracted for analysis (see Table 2 and Figure 1). Eruptions were deemed as tropical if volcanic aerosols were present in significant amounts in both hemispheres.

The Kuwae eruption is included within the analysed eruptions, and is dated to 1452CE. While this year contains the bi-hemispheric deposition from the Kuwae eruption in both volcanic datasets used in this study, it is important to note that Sigl et al. (2013) recently constructed an ice-core record of volcanism that dates the Kuwae eruption to 1459/1459CE, with another, smaller eruption occurring at 1452. For the purposes of this paper, however, Kuwae will be considered as the 1452 deposition event.

We explored anomalous conditions in ENSO, the IOD and Australian rainfall. For ENSO, the period December-February (DJF) was examined using the NINO3.4 index, defined by the averaged sea surface temperature (SST) anomalies between 5N-5S and 170-120W. When analysing the IOD, the July-November (JASON) period was examined



130 due to the IOD's tendency to develop and mature over these months (Weller et al., 2014). The IOD was measured using the Dipole Mode Index (DMI), which subtracts the averaged SST in the EIO (90-110E; 10S-O) from the averaged SST in the WIO (50-70E; 10S-10N).

135 Australian precipitation was processed to find the anomalies of each season and year relative to the long-term mean. Rainfall was also examined over the period JASON. Analyses were conducted on south-eastern Australia (132.5-155E; 27.5-45S) and north-western Australia (110-132.5E; 10-27.5S). The south-east and north-west were chosen for analysis as the effect of the IOD on Australian precipitation is largest in, and potentially limited to, these areas (Ashok et al., 2004).

140 The response of these large-scale modes of variability and rainfall are investigated using an epoch approach. For each major identified eruption, a response was defined by subtracting a reference period (the mean of 5 years pre-eruption) from the eruption year and the six years following eruption individually. A reference period of five years was chosen as it minimised the effect of trends or low-frequency climate variability (Iles et al., 2013). Mode specific graphs (IOD, ENSO, Australian Precipitation) focused on the nine years surrounding eruption (years -2 to 6, with year 0 being the year of eruption). The mean of all six eruptions in each ensemble were calculated for individual years, and then the mean of all ensembles included in each forcing category were compared (CR, 2xG or None).

145

3. Results

150 The global SST response for the CR forcing group shows predominantly surface cooling anomalies (Fig. 2). More specifically, cooling occurs in the Northern Hemisphere from years 0-3, while the south Atlantic, Indian and Pacific oceans show mostly minor warming. An El Nino-like temperature gradient is apparent in years 0,1 and 4, relative to the eruption, despite overall cooling trends. In the Southern Hemisphere, cooling is most pronounced over land masses, particularly Australia and the southern tip of Africa.

155 The DMI response showed a significant pIOD condition one year after a major eruption in all volcanically forced ensembles that persists until year 5, where an abrupt negative IOD phase occurs (Fig. 3). This response can also be seen in Fig. 2, where the EIO region shows larger and more widespread cooling anomalies than the WIO region in years 1, 2 and 4. This response contrasts to the non-volcanically forced ensembles, which show neither a prolonged pIOD nor nIOD condition. The response of the DMI to the largest and smallest eruptions were also extracted. Fig. 4 show the mean DMI response to the 1258 Samalas eruption (257.91 Tg) and the 1600 Huaynaptina eruption (56.59 Tg). Our results show that while both eruptions caused a significant simulated pIOD at year 1, the larger 1258 Samalas eruption 160 persisted with a significant pIOD condition in years 2 and 4, while the 1600 Huaynaptina eruption did not.

165 The mean NINO3.4 multi-volcano response to ensemble forcing showed a statistically significant El-Nino like response for all 6 years following eruption, with a peak at year 3 in both the CR and 2xG ensembles (Fig. 5). The non-volcanically forced ensemble group showed neither a significant El Nino nor La Nina tendency, with the NINO3.4 index remaining within 0.4/-0.4. The index also showed an increase in the intensity and endurance, of post-volcanic El Ninos between the Samalas and Huaynaptina eruptions (Fig. 6). The Samalas eruption was followed by an El Nino that endured for 3 years, from years 1-3, peaking at a NINO3.4 anomaly of 0.68 in year 3, while Huaynaptina peaked at 0.53 in year 2 from an El Nino that endured for 2 years.



170

Fig. 7 shows the mean precipitation response of all volcanically forced ensembles. Substantial precipitation deficits can be seen in the tropics in years 0-2, with a deficit band of decreased precipitation also occurring at approximately 40°S and between 0-40°N in the western Pacific and North Atlantic Oceans. The Southern Hemisphere subtropics appear to have a slight increase in precipitation in years 0-2, most prominently, over Australia and southernmost Africa, while the southern polar region (60-90°S) shows only variable minor precipitation anomalies occurring in all 6 years post eruption. The northern polar area (60-90°N) exhibits a greater response than the south pole in the immediate years following eruption, with moderate cooling anomalies occurring over landmasses.

175

Ensembles with volcanic forcing showed an increase in precipitation over southeast (SE) (Fig. 10) and northwestern (NW) (Fig. 8) Australia between July to November (JASON). Both areas showed predominantly positive anomalies in years 0-5 post-eruption, with the largest response seen between years 0-2. NW Australia (Fig. 8) showed larger positive precipitation anomalies between years 0-2 than SE Australia (Fig. 10) in the CR ensemble mean, and in years 0 and 2 in the 2xG ensemble mean.

180

Comparison of the precipitation anomalies following the Samalas and Huaynaptina eruptions in NW Australia (Fig. 9) showed that the smaller eruption had a delayed and smaller positive precipitation peak, with Samalas peaking in year 0 with an anomaly of 0.23 and Huaynaptina in year 2 at 0.14. While the Huaynaptina eruption also showed a delayed peak in precipitation in SE Australia (Fig 11), the persistence of positive precipitation anomalies exceeded those of the Samalas eruption. Huaynaptina recorded values >0.17 in years 1-2 and a value of 0.12 in year 4, all of which were larger anomalies than the peak of the Samalas eruption at 0.11 in year 1 (Fig. 11).

185

190

4. Discussion and conclusions

Our results suggest that the large-scale IOD and ENSO systems, and Australian rainfall regimes, were all impacted by large tropical eruptions of the Last Millennium.

195

The DMI response simulated in the GISS ensemble following large eruptions is complimentary to previous research conducted by Cheung & Abram (2015) and Maher et al. (2015). The pIOD peak in year 1 (Fig. 3) is consistent with both studies, in which statistically significant pIOD conditions occurred between 6 months to 2 years after an eruption. Cheung & Abram (2015) also found a statistically significant negative condition immediately after eruption at year 0, however this was absent from both Maher et al.'s (2015) results and the CR forcing category in this study. The 2xG category does show a nIOD condition at year 0, but is not believed to be a response to volcanic forcing as a similar nIOD condition can be seen at year -1. The abrupt shift to a negative condition at year 5 was not found in either Cheung & Abram (2015) or Maher et al. (2015)'s results. Both studies found a gradual decrease in DMI from year 1 to years 3-4.

200

205

The smooth transition to a lower DMI following eruptions found by Cheung & Abram (2015) and Maher et al. (2015) contrasts with the abrupt change from a pIOD of approximately 0.13 at year 4, to an nIOD of -0.069 in the CR ensembles and -0.083 in the 2xG ensemble at year 5 (Fig. 3). This inconsistency between studies could be due to the selection of eruptions analysed by each paper. Cheung & Abram (2015) included all eruptions from 850-2005CE recorded on the IVI2 in their analysis. While this encompasses all eruptions analysed here, it also included many

210



smaller eruptions that would likely have dampened the climatic response, a response that has been analysed in previous papers (Zambri & Robock, 2016). Maher et al. (2015) looked at the five largest eruptions from 1880 to present, of which the largest was Pinatubo (1991), measured at 30.10 Tg globally on the IVI2 (Gao et al., 2008). In comparison, our research deals with eruptions of much larger atmospheric loading, ranging from 56.59 to 257.91 Tg. Therefore, the smallest eruption dealt with in this paper is almost double that of the largest in Maher et al.'s (2015) analysis.

The persistence of a high pIOD through to year 5 seen here may result from the larger mean atmospheric sulfate loading imposed. This theory is supported by the comparison between the Samalas and Huaynaptina (Fig. 4) eruptions. Our results showed that while both eruptions caused a significant pIOD at year 1, the larger 1258 Samalas eruption alone persisted with a significant pIOD condition in following years. Further support can be gathered from the comparison between the 2xG and CR ensemble means in fig. 3. Years 0-3 show more extreme values in the 2xG ensemble mean, while years 4-6 show similar values for both forcing categories. Maher et al. (2015) found a similar response, with the two largest eruptions analysed in the paper showing the largest and longest enduring pIOD anomalies. This suggests that larger mean atmospheric sulfate loading can cause not only more persistent, but also more extreme pIOD conditions.

The NINO3.4 response found in this research supports previous studies by Adams et al. (2003), Mann et al. (2005), Emile-Geay et al. (2008), McGregor et al. (2010) and Maher et al. (2015). Fig. 5 shows a very prominent and persistent El-Nino response in all 6 years following eruption, however it lacks the weaker La Nina-like state that was observed 3-6 years after eruption in these previous papers. Spatial maps of our SST (Fig. 2), while dominated by the overall volcanic cooling, show an El Nino-like pattern in the eastern Pacific that is most visible in year 4, but is also distinctive in years 0, 1 and 3. We can therefore conclude that an El Nino-like anomaly was generated in the multimodel mean response in years 0-6 following eruption, despite the overall cooling trend caused by the volcanic aerosols. Comparison of the Samalas and Huaynaptina (Fig. 6) eruptions also suggest that, similar to the DMI, the intensity and endurance of the ENSO response to volcanic forcing increases with increasing mean atmospheric sulfate loading. This once again supports the findings of Maher et al. (2015) that identified a similar pattern.

The positive response of Australian precipitation to volcanic forcing as seen here (Fig. 7, 8 & 10) is in agreement with several papers that identified positive precipitation responses over Australia to large volcanic eruptions (Schneider et al., 2009; Joseph & Zeng, 2011). Our results suggest that the direct precipitation effect of volcanic aerosols override the impact of the IOD on Australian precipitation in the years following large tropical volcanic eruptions. NW Australia (Fig. 8) showed larger positive precipitation anomalies between years 0-2 than SE Australia (Fig. 10) in the CR ensemble mean, and in years 0 and 2 in the 2xG ensemble mean. This could be due to the positive precipitation anomalies that can be generated by combined El Nino and pIOD events in the NW Australian region (Meyers et al., 2007 & Pepler et al., 2014), enhancing the precipitation surplus caused by volcanic aerosols.

The varying response of NW Australia to the Samalas and Huaynaptina eruptions (Fig. 9) also supports the enhancement of the volcanically induced precipitation surplus by combined El Nino and pIOD events. The Samalas eruption was followed by strong and enduring El Nino and pIOD conditions for up to 4 years post volcanism, and showed larger positive precipitation anomalies from years 0-3 than the Huaynaptina eruption, that was accompanied by smaller, shorter-lived El Nino and pIOD conditions. The precipitation surplus to the Samalas eruption in NW and SE Australia also peaked earlier than Huaynaptina, which could be a response to the larger atmospheric sulfate loading.



255 Interestingly, previous papers have not reported a relationship between atmospheric sulfate loading and the peak in precipitation response (Robock & Lui, 1994; Iles et al., 2013; Iles et al., 2015).

260 The precipitation anomalies of SE Australia (Fig. 11) further supports this theory. The response to the Huaynaptina eruption, while peaking later than Samalas, endured longer, and with larger positive anomalies. The effect of strong, combined El Niño and pIOD conditions on SE Australia is significant precipitation deficits (Meyers et al., 2007 & Pepler et al., 2014), and could explain the negative precipitation anomalies that occur in the Samalas response from year 2 onwards, where the combined influence of a strong El Niño and pIOD dampened the positive precipitation response generated by the atmospheric sulfate loading.

265 We note that our study has provided an analysis of climatic response to a set of forcings in a single climate model, which may limit the precise interpretation of responses to eruptions. Overall, volcanic aerosols remain an understudied climatic forcing such that the timing, magnitude and spatial footprint of past eruptions remains uncertain (Colose et al., 2016). In addition to uncertainties around the fundamental physical forcings, limitations still exist in the implementation of volcanic eruptions in climate models (Colose et al., 2016; Zambri et al., 2017). For example, Colose et al. (2016) suggest that improvements in model representations of volcanic particle size may improve the accuracy of model 270 simulations. Furthermore, LeGrande et al. (2016) note that the chemistry and composition of a volcanic plume affects its climatic impact, which requires realistic representation in climatic models. Overall, these limitations in modeling eruptions and the idealised approach adopted here may mean that impacts simulated do not precisely match those of the proxy record.

275 In summary, this paper aimed to identify the impact of large, tropical volcanism on the ENSO, IOD and Australian rainfall. Results showed an El Niño and pIOD response in the immediate years following eruption, accompanied by positive precipitation anomalies over SE and NW Australia. The positive precipitation anomalies suggest that volcanic aerosol cooling dominates the precipitation response, rather than the effect of ENSO or IOD, despite aerosols also proving to be an important influence on these large scale modes. Although this study focused on Australian rainfall regimes and its main climatic drivers, this approach can be applied for exploring the impact of time-evolving forcings, 280 such as volcanism, in other regions.

Acknowledgements

285 We thank NASA GISS for institutional support. S.C.L. is funded through Australian Research Council (ARC) DECRA Fellowship (DE160100092) and additional funding is provided through the Australian Research Council Centre of Excellence for Climate System Science (CE110001028). We also thank the NASA MAP programme for continued support of A.N.L. Resources supporting this work were provided by the NASA High-End Computing (HEC) Program through the NASA Center for Climate Simulation (NCCS) at Goddard Space Flight Center.

290

References

295 Adams, J. B., Mann, M. E., and Ammann C. M.: Proxy evidence for an El Niño-like response to volcanic forcing, *Nature*, 426, 274-278, doi:10.1038/nature02101, 2003.

Anchukaitis, K. J., Buckley, B. M., Cook, E. R., Cook, B. I., Arrigo, R. D. D., and Ammann, C. M.: Influence of volcanic eruptions on the climate of the Asian monsoon region: *Geophys. Res. Lett.*, 37, L22703, doi: 10.1029/2010GL044843, 2010.



- 300 Ashok, K., Guan, Z., Saji, N. H., and Yamagata, T.: Individual and combined influences of ENSO and the Indian Ocean Dipole on the Indian summer monsoon, *J. Clim.*, 17, 3141–3155, doi: 10.1175/1520-0442(2004)017<3141:IAOIE>2.0.CO;2, 2004.
- Cheung, A. N. and Abram, N. J.: Indian Ocean Dipole variability during the Late 13th C, Final Report for EMSC3050 Special Topics Research Project, 2016.
- 305 Clement, A., Seager, R., Cane, M. A. and Zebiak, S. E.: An ocean dynamical thermostat, *J. Clim.*, 9, 2190–2196, doi:10.1175/1520-0442(1996)009<2190:AODT>2.0.CO;2, 1996.
- Colose, C. M., LeGrande, A. N. and Vuille, M.: Hemispherically asymmetric volcanic forcing of tropical hydroclimate during the last millennium, *Earth Syst. Dyn.*, 7, 681–696, doi:10.5194/esd-7-681-2016, 2016.
- 310 Crowley, T. and Unterman, M.: Technical details concerning development of a 1200 yr proxy index for global volcanism, *Earth Syst. Sci. Data*, 5, 187–197, doi:10.5194/essd-5-187-2013, 2013.
- Ding, Y., Carton, J. A., Chepurin, G. A., Stenchikov, G., Robock, A., Sentman, L. T. and Krasting, J. P.: Ocean response to volcanic eruptions in Coupled Model Intercomparison Project 5 simulations, *J. Geophys. Res. Oceans*, 119, 5622–5637, doi:10.1002/2013JC009780, 2014.
- 315 Driscoll, S., Bozzo, A., Gray, L. J., Robock, A., and Stenchikov, G.: Coupled Model Intercomparison Project 5 (CMIP5) simulations of climate following volcanic eruptions, *J. Geophys. Res.*, 117, doi:10.1029/2012JD017607, 2012.
- Emile-Geay, J., Seager, R., Cane, M. A., Cook, E. R., and Haug, G. H.: Volcanoes and ENSO over the Past Millennium, *J. Clim.*, 21, 3134–3148, doi: 10.1175/2007JCLIM1884.1, 2008.
- 320 Gao, C., Robock, A., and Ammann, C. M.: Volcanic forcing of climate over the past 1500 years: An improved ice core-based index for climate models, *J. Geophys. Res.*, 113, D23111, doi:10.1029/2008JD010239, 2008.
- 325 Gillett N. P., Weaver, A. J., Zwiers, F. W., and Wehner, M. F.: Detection of volcanic influence on global precipitation, *Geophys. Res. Lett.*, 31, L12217. doi:10.1029/2004GL020044, 2004.
- Gu, G., and Adler, R.: Large-scale, inter-annual relations among surface temperature, water vapour and precipitation with and without ENSO and volcano forcings, *International J Climatology*, 32, 1782–1791, doi: 10.1002/joc.2393, 2011.
- 330 Iles, C. E., Hegerl, G. C., and Schurer, A. P.: Volcanic eruptions and the global hydrological cycle, *Pages*, 23:2, 56–57, 2015.
- Iles, C. E., Hegerl, G. C., Schurer, A. P., and Zhang, X.: The effect of volcanic eruptions on global precipitation, *J Geophys. Res. Atmos.*, 118, 8770–8786, doi:10.1002/jgrd.50678, 2013.
- 335 Joseph, R., and Zeng, N.: Seasonally modulated tropical drought induced by volcanic aerosol, *J Clim.*, 24, 2045 – 2060, doi: 10.1175/2009JCLI3170.1, 2011.
- LeGrande, A. N., Tsigaridis, K., and Bauer, S. E.: Role of atmospheric chemistry in the climate impacts of stratospheric volcanic injections, *Nat. Geosci.*, 9, 652–655, doi: 10.1038/NGEO2771, 2016.
- 340 Lewis, S. C. and LeGrande, A. N. Stability of ENSO and its tropical Pacific teleconnections over the Last Millennium, *Clim. Past*, 11, 1347–1360, doi:10.5194/cp-11-1347-2015, 2015.
- Lewis, S. C., and Karoly, D. J.: Assessment of forced responses of the Australian Community Climate and Earth System Simulator (ACCESS) 1.3 in CMIP5 historical detection and attribution experiments, *Aus Meteorological and Oceanographic Journal*, 64, 5–20, doi: 10.22499/2.6402.001, 2014.
- 345 Maher, N., McGregor, S., England, M. H., and Gupta, A. S.: Effect of volcanism on tropical variability, *Geophys. Res. Lett.*, 42, 6024–6033, doi:10.1002/2015GL064751, 2015.
- 350 Mann, M., Cane, M., Zebiak, S., and Clement, A.: Volcanic and solar forcing of the tropical Pacific over the past 1000 years, *J Clim.*, 18, 447–456, doi: 10.1175/JCLI-3276.1, 2005.
- Meyers, G., McIntosh, P., Lidia, L., and Pook, M.: The Years of El Nino, La Nina and Interactions with the Tropical Indian Ocean, *J Clim.*, 20, 2972–2880, doi: 10.1175/JCLI4152.1, 2007.
- 355 McGregor, S. and Timmermann, A.: The effect of explosive tropical volcanism on ENSO, *J. Clim.*, 24, 2178–2191, doi: 10.1175/2010JCLI3990.1, 2011.
- 360 McGregor, S., Timmermann, A., and Timm, O.: A unified proxy for ENSO and PDO variability since 1650, *Clim. Past*, 5, 1–17, doi:10.5194/cp-6-1-2010, 2010.
- Oman, L., Robock, A., Stenchikov, G., Schmidt, G. A., and Ruedy, R.: Climatic response to high-latitude volcanic eruptions, *J Geophys. Res.*, 110, D13103, doi:10.1029/2004JD005487, 2005.



- 365 Pausata, F. S. R., Chafik, L., Caballero, R., and Battisti, D. S.: Impact of high-latitude volcanic eruptions on ENSO and AMOC, *PNAS*, 112:45, 13784-13788, doi:10.1073/pnas.1509153112, 2015.
- Pepler, A., Timbal, B., Rakich, C. and Coutts-Smith, A.: Indian Ocean Dipole overrides ENSO's influence on cool season rainfall across the Eastern Seaboard of Australia, *J Clim.*, 27, 3816-3826, doi: 10.1175/JCLI-D-13-00554.1, 2014.
- Predybaylo, E., Stenchikov, G. L., Wittenberg, A. T., and Zeng, F.: Impacts of a Pinatubo-size volcanic eruption on ENSO, *J Geophys. Res. Atmos.*, 122, 925-947, doi:10.1002/2016JD025796, 2017.
- 370 Robock, A.: Volcanic eruptions and climate, *Reviews Geophys.*, 38, 191-219, doi: 8755-1209/00/1998RG000054, 2000.
- Robock A and Liu, Y.: The volcanic signal in Goddard Institute for Space Studies three-dimensional model simulations, *J Clim.*, 7, 44-55, doi: 10.1175/15200442(1994)007<0044:TVSIGI>2.0.CO;2, 1994.
- 375 Roxy, M., Gualdi, S., Drbohlav, H. L., and Navarra, A.: Seasonality in the relationship between El Nino and the Indian Ocean dipole, *Clim. Dynam.*, 37, 221-236, doi: 10.1007/s00382-010-0876-1, 2011.
- Schmidt, G. A., Kelley, M., Nazarenko, L., Ruedy, R., Russel, G., Aleinov, I., et al.: Configuration and assessment of the GISS ModelE2 contributions to the CMIP5 archive, *J. Advances in Modeling Earth Systems*, 6:1, 141-184, doi: 10.1002/2013MS000265, 2014.
- 380 Schneider, D. P., Ammann, C. M., Otto-Bliesner, B. L., and Kaufman, D. S.: Climate response to large, high-latitude and low-latitude volcanic eruptions in the Community Climate System Model, *J Geophys. Res.*, 114, D15101, doi:10.1029/2008JD011222, 2009.
- 385 Self, S., Rampino, M. R., Zhao, J., and Katz, M. G.: Volcanic aerosol perturbations and strong El Nino events: No general correlation, *Geophys Res Lett*, 24, 1247-1250, 1997.
- Shindell, D., Schmidt, G., Mann, M., and Faluvegi, G.: Dynamic winter climate response to large tropical volcanic eruptions since 1600, *J Geophys. Res.*, 109, D05104, doi:10.1029/2003JD004151, 2004.
- 390 Sigl, M., McConnell, J. R., Layman, L., Maselli, O., McGwire, K., Pasteris, D., Dahl-Jensen, D., Steffensen, J. P., Vinther, B., Edwards, R., Mulvaney, R., and Kipfstuhl, S.: A new bipolar ice core record of volcanism from WAIS Divide and NEEM and implications for climate forcing of the last 2000 years, *J. Geophysic Res. Atmos.*, 118:3, 1151-1169, doi: 10.1029/2012JD018603
- Soden, B., Wetherald, R., Stenchikov, G., and Robock, A.: Global cooling after the eruption of Mount Pinatubo: A test of climate feedback by Water Vapour, *Science*, 296, 727-730, doi: 10.1126/science.296.5568.727, 2002.
- 395 Stenchikov, G., Hamilton, K., Stouffer, R. J., Robock, A., Ramaswamy, V., Santer, B., and Graf, H. F.: Arctic Oscillation response to volcanic eruptions in the IPCC AR4 climate models, *J. Geophys Res*, 111, D07107, doi:10.1029/2005JD006286, 2006.
- Stenchikov, G., Delworth, T. L., Ramaswamy, V., Stouffer, R. J., Wittenberg, A., and Zeng, F.: Volcanic signals in oceans, *J Geophys. Res.*, 144, doi: 10.1029/2008JD011673, 2009.
- 400 Stevenson, S., Otto-Bliesner, B., Fasullo, J., and Brady, E.: El Nino like hydroclimate response to last millennium volcanic eruptions, *J Clim.*, 29:8, 2907-2921, doi: 10.1175/JCLI-D-15-0239.1, 2016.
- Taylor, K. E., Stouffer, R. J., and Meehl, G. A.: An overview of CMIP5 and the experiment design, *BAMS*, 485-498, doi:10.1175/BAMS-D-11-00094.1, 2012.
- 405 Timmreck C, Graf, H. F., Zanchettin, D., Hagemann, S., Kleinen, T., and Kruger, K.: Climate response to the Toba eruption: regional changes, *Quat Int*, 258, 30-44, doi: 10.1016/j.quaint.2011.10.008, 2012.
- 410 Ummenhofer, C., England, M., McIntosh, P., Meyers, G., Pook, M., Risbey, J., Gupta, A., and Taschetto, A.: What causes southeast Australia's worst droughts?, *Geophys. Res. Lett.*, 36, L04706, doi:10.1029/2008GL036801, 2009.
- Wahl, E. R., Diaz, H. F., Smerdon, J. E. and Ammann, C. M.: Late winter temperature response to large tropical volcanic eruptions in temperate western North America: Relationship to ENSO phases, 122, 238-250, doi: 10.1016/j.gloplacha.2014.08.005, 2014.
- 415 Weller, E., Cai, W., Du, Y., and Min, S-K.: Differentiating flavors of the Indian Ocean Dipole using dominant modes in tropical Indian Ocean rainfall, *Geophys. Res. Lett.*, 41, 8978-8986, doi:10.1002/2014GL062459, 2014.
- 420 Wielicki, B., Wong, T., Allen, R., Slingo, A., Kiehl, J., Soden, B., Gordon, C., Miller, A., Yang, S., Randall, D., Robertson, F., Susskind, J., and Jacobowitz, H.: Evidence for large decadal variability in the tropical mean radiative energy budget, *Science*, 295, 841-844, doi: 10.1126/science.1065837, 2002.
- Zambri, B., and Robock, A.: Winter warming and summer monsoon reduction after volcanic eruptions in Coupled Model Intercomparison Project 5 (CMIP5) simulations, *Geophys. Res. Lett.*, 4320, 10,920-10,928, doi: 10.1002/2016GL070460, 2016.



425 Zambri, B., Slawinska, J., Robock, A., and LeGrande, A. N.: Northern Hemisphere winter warming and summer monsoon reduction after volcanic eruptions over the last millennium, *J. Geophys. Res. Atmos.*, in press, doi:10.1002/2017JD026728, 2017.

Zanchettin, D., Timmreck, C., Graf, H. F., Rubino, A., Lorenz, S., Lohmann, K., Krüger, K., and Jungclaus, J. H.: Bi-decadal variability excited in the coupled ocean-atmosphere system by strong tropical volcanic eruptions, *Clim. Dyn.*, 39, 419–444, 2012.

430

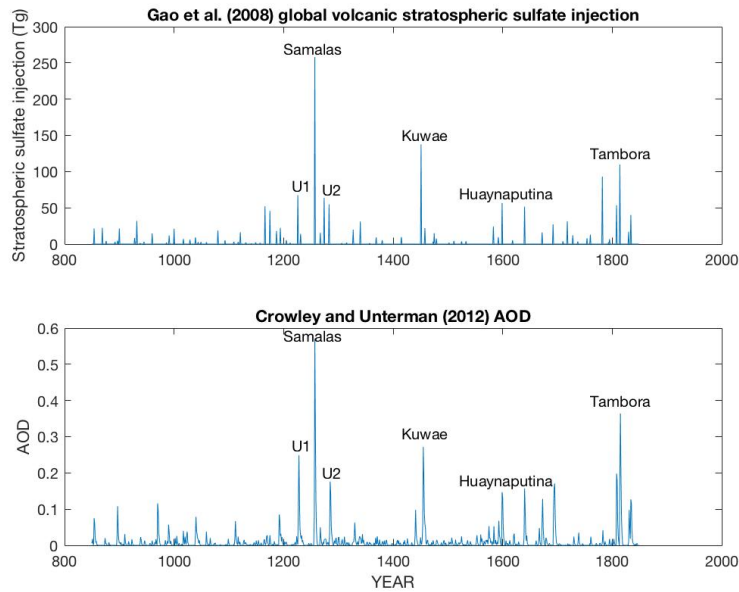
Volcanic forcing	Ensembles
None	E4rhLMgTs, E4rhLMgTnck, E4rhLMgTKk, E4rhLMgTk
Crowley & Unterman (2012)	E4rhLMgTncck, E4rhLMgTKck, E4rhLMgTcs, E4rhLMgTck
2 x Gao et al. (2008)	E4rhLMgTKgk

Table 1: Volcanic forcing used for ensembles.

Eruption Name	Year	Tg
Samalas	1258	257.91
Kuwae	1452	137.50
Tambora	1815	109.72
Unknown 1	1227	67.52
Unknown 2	1275	63.72
Huaynaputina	1600	56.59

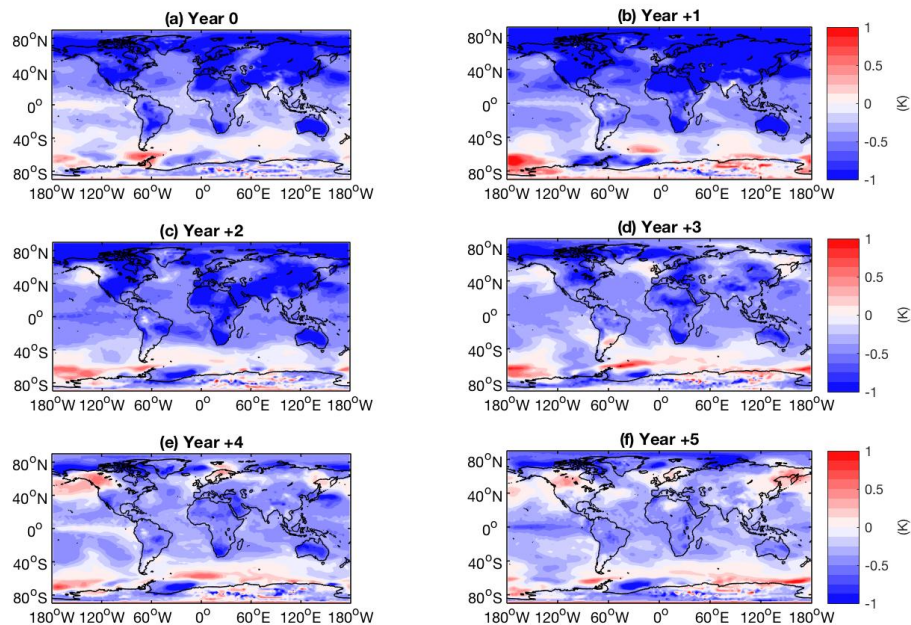
435

Table 2: The six largest tropical eruptions of the last millennium and their total global stratospheric sulfate injection (Tg) as recorded by Gao et al. (2008), revised in 2012.



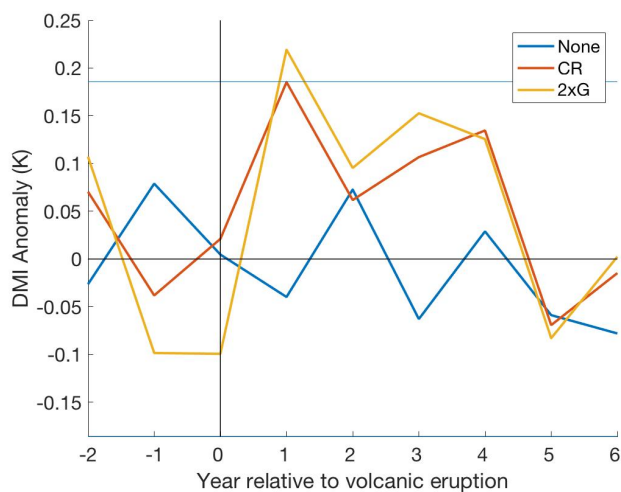
440

Fig 1: Timeseries of volcanic forcing from Gao et al. (2008) (upper) and Crowley and Unterman (2012) (lower). The specific subset of volcanic eruptions investigated is labelled.

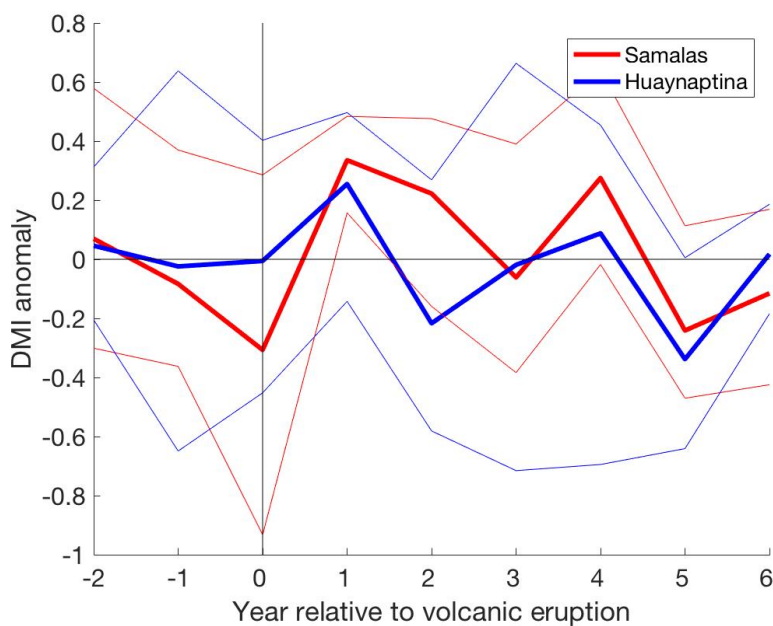


445

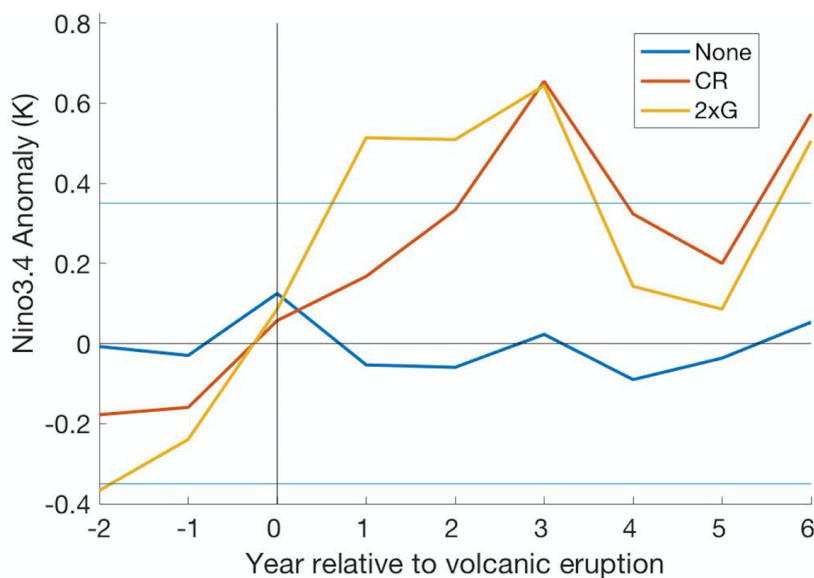
Fig 2: Global SST anomalies (K) in response to the Crowley (CR) forcings, showing multi-model mean response averaged across all analysed eruptions for years 0 to +5 after eruption



450 **Fig 3: Multi-model and multi-volcano mean DMI (Dipole Mode Index) response to CR, 2xG and None ensemble forcing groups over July–November (JASON). Significance was tested using the 0.6 standard deviation threshold (horizontal blue lines), and by comparing the CR and 2xG ensembles to those without volcanic forcing.**

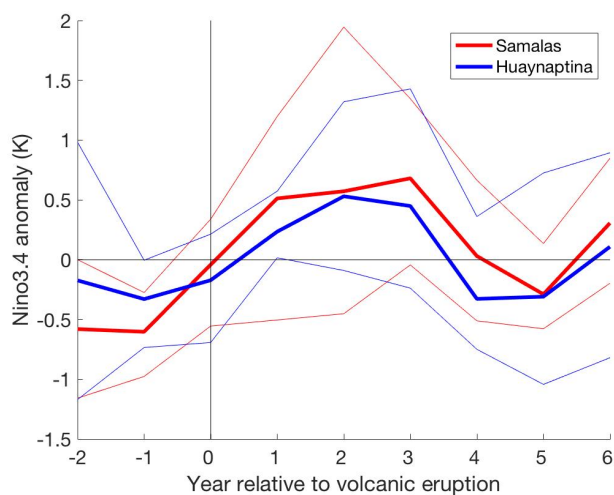


455 **Fig 4: Mean DMI response across all volcanic ensembles to the largest (1258 Samalas) and smallest (1600 Huaynaptina) eruptions analysed. The bold lines represent the mean of all volcanic ensembles to each eruption, and the fainter lines represent the 90th and 10th percentile.**



460

Fig 5: Multi-model and multi-volcano mean NINO3.4 response to CR, 2xG and None ensemble forcing groups over DJF. Significance was tested using the 0.6 standard deviation threshold (horizontal blue lines), and by comparing the CR and 2xG ensembles to those without volcanic forcing.



465

Fig 6: Mean NINO3.4 response across all volcanic ensembles to the largest (1258 Samalas) and smallest (1600 Huaynaptina) eruptions analyzed. The bold lines represent the mean of all volcanic ensembles to each eruption, and the fainter lines represent the 90th and 10th percentile.

470

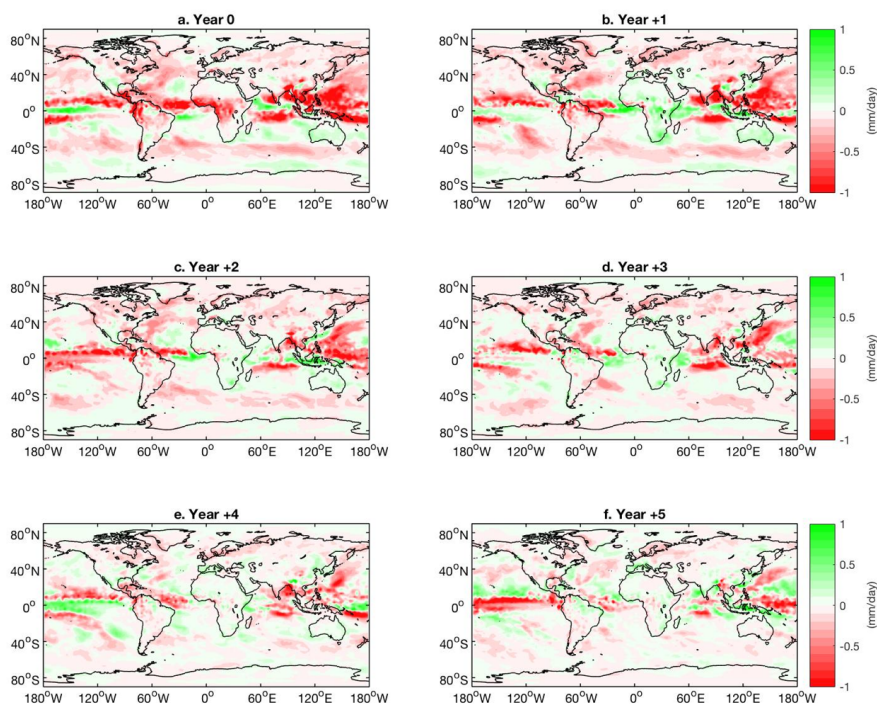


Fig 7: Global precipitation anomalies (mm/day) in response to the Crowley and Unterman (CR) forcings, showing multi-model mean responses averaged across all analysed eruptions for years 0 to +5 after eruption.

475

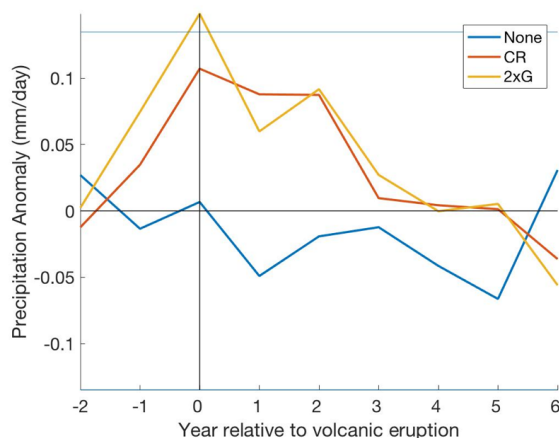


Fig 8: Mean NW Australian precipitation (mm/day) response to CR, 2xG and None forcing ensemble groups in the eight years surrounding eruption. Significance was tested using the 0.6 standard deviation threshold (horizontal blue lines), and by comparing the CR and 2xG ensembles to those without volcanic forcing.

480

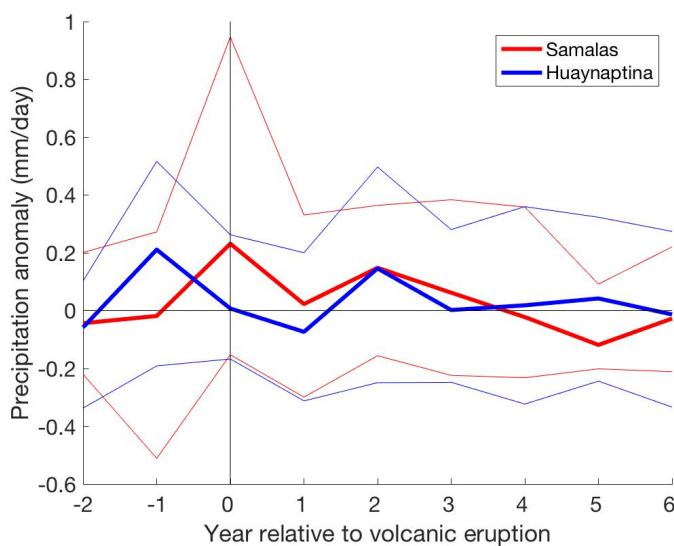
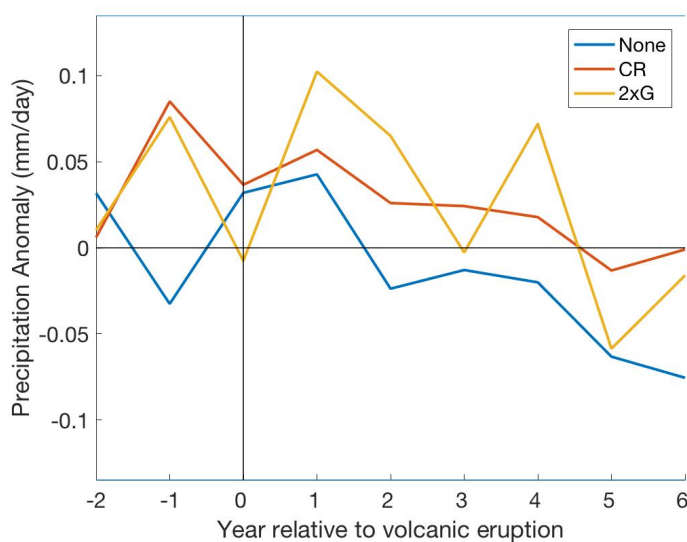


Fig 9: Mean NW Australian precipitation (mm/day) response across all volcanic ensembles to the largest (1258 Samalas) and smallest (1600 Huaynaptina) eruptions analysed. The bold lines represent the mean of all volcanic ensembles to each eruption, and the fainter lines represent the 90th and 10th percentile.



485

Fig 10: Australian precipitation (mm/day) response to CR, 2xG and None forcing ensemble groups in the eight years surrounding eruption. Significance was tested using the 0.6 standard deviation threshold (horizontal blue lines), and by comparing the CR and 2xG ensembles to those without volcanic forcing.

490

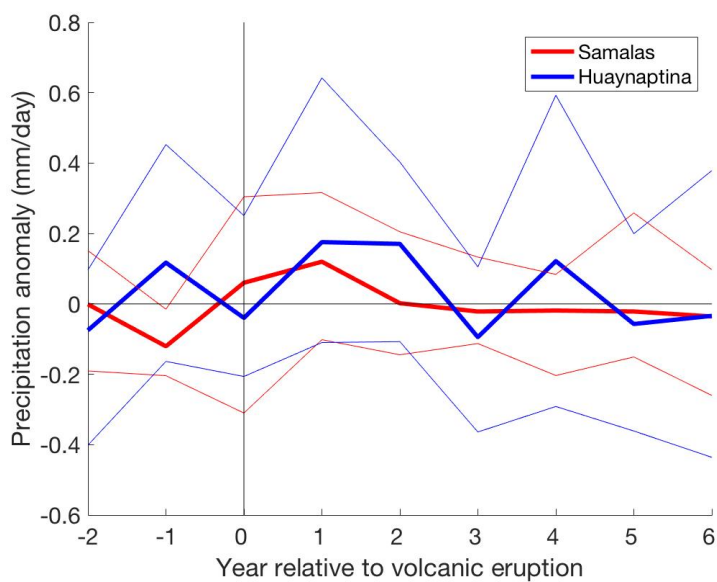


Fig 11: Mean SE Australian precipitation (mm/day) response across all volcanic ensembles to the largest (1258 Samalas) and smallest (1600 Huaynaptina) eruptions analysed. The bold lines represent the mean of all volcanic ensembles to each eruption, and the fainter lines represent the 90th and 10th percentile.

495